Multiterminal spin-dependent transport in ballistic carbon nanotubes

Audrey Cottet, Chéryl Feuillet-Palma, and Takis Kontos
Ecole Normale Supérieure, Laboratoire Pierre Aigrain, 24 rue Lhomond, 75231 Paris Cedex 05, France and CNRS UMR8551, Laboratoire associé aux universités Pierre et Marie Curie et Denis Diderot, France
(Received 28 November 2008; published 20 March 2009)

We study theoretically nonlocal spin transport in a ballistic carbon nanotube contacted to two ferromagnetic leads and two normal-metal leads. When the magnetizations of the two ferromagnets are changed from a parallel to an antiparallel configuration, the circuit shows a hysteretic behavior which is specific to the few-channel regime. In the coherent limit, the amplitude of the magnetic signals is strongly enhanced due to resonance effects occurring inside the nanotube. Our calculations pave the way for experiments on low-dimensional nonlocal spin transport, which should give results remarkably different from the experiments realized so far in the multichannel diffusive incoherent regime.

DOI: 10.1103/PhysRevB.79.125422 PACS number(s): 73.23.Ad, 85.75.−d

I. INTRODUCTION

Nonlocal electric effects have been observed since the early days of mesoscopic physics, e.g., in metallic circuits.[1,2] This fact is related to the primarily nonlocal nature of electronic wave functions in quantum coherent conductors. The spin degree of freedom has raised little attention in this context, although its control and detection are among the major challenges of nanophysics, nowadays. Nonlocal spin signals have been studied for multiterminal metallic conductors,[3–6] semiconductors,[7] and graphene[8] in the multichannel diffusive incoherent (MDI) regime. It has been found that a nonequilibrium spin accumulation induced by a ferromagnet into a given conductor can be detected as a voltage across the interface between this conductor and another ferromagnet.[9] However, to our knowledge, spin-dependent nonlocal effects have not been investigated in the coherent regime so far.

Carbon-nanotube (CNT) based circuits are appealing candidates for observing a nonlocal, spin-dependent, and coherent behavior of electrons. First, electronic transport in CNTs can reach the few-channel ballistic regime, as suggested by the observation of Fabry-Perot-type interference patterns.[10] Second, spin injection has already been demonstrated in CNTs connected to two ferromagnetic leads (see Ref. 11 for a review). Third, nonlocal voltages have been observed in CNTs contacted to four normal-metal leads,[12] which suggests that electrons can propagate in the nanotube sections below the contacts. The study of nonlocal spin transport in CNTs has recently triggered some experimental efforts.[13,14] However, a theoretical insight on this topic is lacking. Some major questions to address are what are the signatures of a nonlocal and spin-dependent behavior of electrons in a nanoconductor, and to which extent these signatures are specific to the coherent regime or the few-channels case.

In this paper, we study the behavior of a CNT with two normal-metal (N) leads and two ferromagnetic (F) leads magnetized in collinear directions. Two leads are used as source and drain to define a local conductance G^c and the other two are used to probe a nonlocal voltage V^c outside the classical current path. We consider two different setups which differ on the positions of the F leads. Setup (a) corresponds to the standard geometry used for the study of the MDI limit. In setup (b), the two F leads play the role of the voltage probes so that no magnetic response is allowed in the MDI limit. We mainly focus on the coherent regime, using a scattering description with two transverse modes to account for the twofold orbital degeneracy commonly observed in CNTs.[15] This minimal description is appropriate at low temperatures and bias voltages. We take into account both the spin polarization of the tunneling probabilities at the ferromagnetic contacts and the spin dependence of interfacial phase shifts (SDIPS) which has been shown to affect significantly spin-dependent transport in the two-terminal case.[16–18] This approach leads to strong qualitative differences with the MDI case. In particular, we find a magnetic signal in the conductance G^c of setups (a) and (b), which would not occur in the MDI limit. We also predict an unprecedented magnetic signal in V^c for setup (b). We find that these effects already arise in the incoherent few-channel regime. However, they are much stronger in the coherent case due to resonances which occur inside the CNT. These resonances make the circuit sensitive to the SDIPS, which can furthermore enhance the amplitude of the magnetic signals.

This paper is organized as follows: Sec. II defines setups (a) and (b), Sec. III discusses the MDI limit, Sec. IV focuses on the coherent four-channel (CFC) scattering description, Sec. V presents an incoherent four-channel (IFC) description, Sec. VI discusses the experimental results presently available, and Sec. VII concludes.

II. DEFINITION OF SETUPS (A) AND (B)

In this article, we consider a central conductor (CC) connected to an ensemble $\mathcal{L}$ of two ferromagnetic (F) and two normal-metal (N) reservoirs. We study the two configurations presented in Fig. 1. In both cases, lead 1 is connected to a bias voltage source V_b, lead 2 is connected to ground, whereas leads 3 and 4 are left floating. The only difference between setups (a) and (b) is the position of the two F leads. These F leads can be magnetized in parallel ($c=P$) or antiparallel ($c=\mathrm{AP}$) configurations. We will study the conductance $G^c=\partial I_1^c/\partial V_b$ between contacts 1 and 2 and the voltage drop V^c between leads 3 and 4. The dependence of these quantities on the magnetic configuration c of the ferromag-

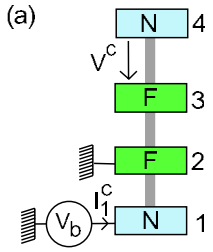

model	MG≠0	V^P≠0	MV≠0
MDI	no	yes	yes
IFC	yes$^{\Diamond,\times}$	yes	yes$^{\times}$
CFC	yes	yes	yes

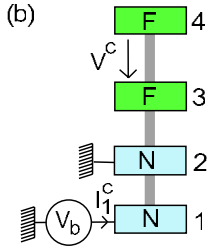

model	MG≠0	V^P≠0	MV≠0
MDI	no	no	no
IFC	yes$^{+,\times}$	yes^{+}	yes$^{+,\times}$
CFC	yes	yes^{+}	yes^{+}

$^{\Diamond}$ if at least one of the contacts scatter the K and K' modes differently

$^{+}$ if contacts 1 and 2 scatter the K and K' modes differently

$^{\times}$ these signals are generally much smaller than in the CFC case

FIG. 1. (Color online) Left: the two types of circuits [setups (a) and (b)] studied in this article. The central conductor (represented with the gray bar) is contacted to two normal-metal leads N and two ferromagnetic leads F, which can be magnetized in parallel ($c=P$) or antiparallel ($c=\mathrm{AP}$) configurations. The only difference between setups (a) and (b) is the position of the two F leads. Contacts 1 and 2 are used as source and drain to measure a local conductance G^c, and contacts 3 and 4 are used to probe a nonlocal voltage V^c outside the classical current path. Right: tables presenting the behaviors of setups (a) and (b) in various regimes. We study the existence of the signals $MG=(G^P-G^{\mathrm{AP}})/G^P$, V^P, and $MV=(V^P-V^{\mathrm{AP}})/V_b$. We compare the predictions of the CFC model in Sec. IV, the IFC model of Sec. V, and the MDI model in Sec. III.

netic electrodes can be characterized with the magnetic signals $MG=(G^P-G^{\mathrm{AP}})/G^P$ and $MV=(V^P-V^{\mathrm{AP}})/V_b$.

III. MULTICHANNEL DIFFUSIVE INCOHERENT LIMIT

We first briefly discuss the behavior of setups (a) and (b) in the MDI regime. This case has been thoroughly investigated, in relation with experiments in which the CC is a metallic island.[3–6] For a theoretical description of this regime, one can use spin currents and a spin-dependent electrochemical potential μ_σ which obey a local spin-dependent Ohm's law, provided the mean-free path in the sample is much shorter than the spin-flip length. We refer the reader to Ref. 19 for a detailed justification of this approach from the Boltzmann equations and to Ref. 20 for an overview of this field of research. In this section, we summarize the behaviors expected for setups (a) and (b) in the MDI limit (see the Appendix for a short derivation of these results from a resistors model). A finite current between leads 1 and 2 can lead to a spin accumulation (i.e., $\mu_\uparrow \neq \mu_\downarrow$) in the CC if lead 1 or 2 is ferromagnetic because spins are injected into and extracted from the CC with different rates in this case. The spin accumulation diffuses along the CC beyond lead 2 and reaches leads 3 and 4, provided the spin-flip length is sufficiently long. Then, leads 3 and 4 can be used to detect the spin accumulation provided one of them is ferromagnetic. Indeed, a local unbalance $\mu_\uparrow \neq \mu_\downarrow$ in the CC will produce a voltage drop between the floating lead $j \in \{3,4\}$ and the CC if j is ferromagnetic (these voltage drops aim at equilibrating the spin currents between the CC and the ferromagnetic contact). One can thus conclude that in setup (a) a spin accumulation occurs when $V_b \neq 0$, which leads to $V^c=V^3-V^4 \neq 0$. In contrast, one finds $V^c=0$ in setup (b) because a current flow between N leads 1 and 2 cannot produce any spin accumulation. For completeness, we also mention that in the MDI limit, one finds $G^P=G^{\mathrm{AP}}$ for both setups (a) and (b), due to the fact that leads 3 and 4 are left floating (see the Appendix). The table in Fig. 1 summarizes these results.

IV. COHERENT FOUR-CHANNEL LIMIT

A. General scattering description

In this section, we study the case where the CC is a ballistic CNT allowing coherent transport. The observation of Fabry-Perot-type interference patterns[10] suggests that it is possible, with certain types of metallic contacts, to neglect electronic interactions inside CNTs. We thus use a Landauer-Büttiker scattering description.[21] We take into account two transverse modes $p \in \{K,K'\}$ to account for the twofold orbital degeneracy commonly observed in CNTs.[15] Each transverse mode has two spin submodes $\sigma \in \{\uparrow,\downarrow\}$ defined collinearly to the polarization of the F leads. This gives four channels $m=(p,\sigma)$ in total. We assume that spin is conserved upon scattering by the CNT/lead interfaces and upon propagation along the CNT. This requires, in particular, that the magnetization direction can be considered as uniform in the four F leads and that spin-orbit coupling and spin-flip effects can be neglected inside the CNT and upon interfacial scattering. For simplicity, we also assume that the transverse index p is conserved inside the CNT. In the linear regime, the average current through lead j writes as

$$I_j^c = \sum_k G_{jk} V_k^c \tag{1}$$

with

$$G_{jk} = G_K \left[4\delta_{jk} - \sum_m |S_{jk}^m|^2 \right], \tag{2}$$

$G_K=e^2/h$, and S_{jk}^m the scattering amplitude from lead k to lead j for electrons of channel m. Equation (1) involves the electrostatic potential V_k^c of lead k (we assume that the leads are in local equilibrium so that each one has a single chemical potential for both spin directions). Note that G_{jk} and S_{jk}^m implicitly depend on the configuration c of the ferromagnetic electrodes. In this section, we calculate G^c and V^c by using the general notations of Fig. 2 for the scattering amplitudes. The phase shift δ_{jk} acquired by electrons along the CNT from contacts j to k can be considered as independent of m, with $\delta_{jk}=\delta_{kj}$.[22] In practice, δ_{12}, δ_{23}, and δ_{34} can be tuned using local gate voltage electrodes to change the electronic wave vector in the different CNT sections.[23] We will thus

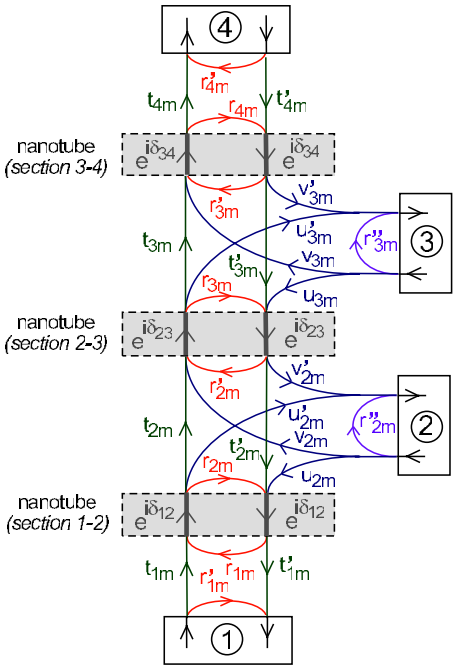

FIG. 2. (Color online) Scheme representing the notations used for the scattering amplitudes of channel m in setups (a) and (b). The rectangles with full lines represent the different leads, and the dashed rectangles represent the nanotube sections between those leads. We note δ_{jk} the phase shift acquired by electrons while propagating along the nanotube between contacts j and k. At this stage, we use $\delta_{jk}=\delta_{kj}$, but we keep $t_{jm}\neq t'_{jm}$, $u_{jm}\neq u'_{jm}$, and $v_{jm}\neq v'_{jm}$ for transparency of the calculation.

study the signals G^c, V^c, MG, and MV as a function of these phases. The calculation of the voltage drop V^c requires to determine V_3^c and V_4^c from $\langle I_3\rangle=\langle I_4\rangle=0$. This yields

$$\frac{V^c}{V_b}=\frac{G_{41}G_{32}-G_{42}G_{31}}{G_{34}G_{43}-G_{33}G_{44}} \tag{3}$$

and

$$G^c/G_K=G_{11}+[G_{13}(G_{44}G_{31}-G_{41}G_{34})+G_{14}(G_{41}G_{33}-G_{31}G_{43})]/[G_{34}G_{43}-G_{33}G_{44}]. \tag{4}$$

Using the notations of Fig. 2, the elements $|S_{jk}^m|$ occurring in Eq. (3) through the coefficients G_{jk} of Eq. (2) can be calculated as

$$|S_{41}^m|=|D_m^{-1}t_{1m}t_{2m}t_{3m}t_{4m}| \tag{5}$$

$$|S_{31}^m|=|D_m^{-1}t_{1m}t_{2m}||u'_{3m}+r_{4m}(t_{3m}v'_{3m}-r'_{3m}u'_{3m})e^{i2\delta_{34}}| \tag{6}$$

$$|S_{42}^m|=|D_m^{-1}t_{3m}t_{4m}||v_{2m}+r_{1m}(t_{2m}u_{2m}-r_{2m}v_{2m})e^{i2\delta_{12}}| \tag{7}$$

$$S_{32}^m=S_{31}^mS_{42}^m/S_{41}^m \tag{8}$$

$$|S_{34}^m|=|D_m^{-1}t'_{4m}||v'_{3m}(1-r_{1m}r_{2m}e^{i2\delta_{12}})+e^{i2\delta_{23}}(r'_{2m}+r_{1m}e^{i2\delta_{12}}[t_{2m}t'_{2m}-r_{2m}r'_{2m}])(t'_{3m}u'_{3m}-r_{3m}v'_{3m})| \tag{9}$$

and

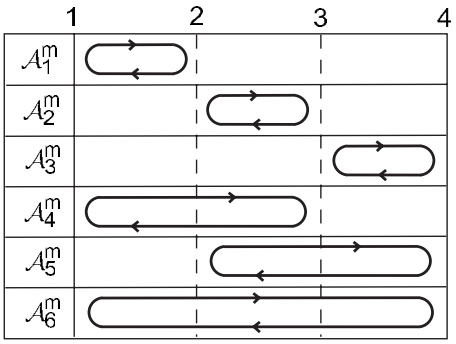

FIG. 3. Scheme representing different resonances (noted $\mathcal{A}_i^m$) which can occur in setups (a) and (b) when $t_{2[3],m}=t'_{2[3],m}=0$ or 1. The upper numbers indicate the position of contacts 1, 2, 3, and 4.

$$|S_{43}^m|=|D_m^{-1}t_{4m}||v_{3m}[1-r_{1m}r_{2m}e^{i2\delta_{12}}]+e^{i2\delta_{23}}[r'_{2m}+r_{1m}e^{i2\delta_{12}}(t_{2m}t'_{2m}-r_{2m}r'_{2m})][t_{3m}u_{3m}-r_{3m}v_{3m}]| \tag{10}$$

with

$$D_m=[(1-r_{1m}r_{2m}e^{i2\delta_{12}})(1-r'_{2m}r_{3m}e^{i2\delta_{23}})(1-r'_{3m}r_{4m}e^{i2\delta_{34}})]-t_{2m}t'_{2m}r_{1m}r_{3m}(1-r'_{3m}r_{4m}e^{i2\delta_{34}})e^{i2(\delta_{12}+\delta_{23})}-t_{3m}t'_{3m}r'_{2m}r_{4m}(1-r_{1m}r_{2m}e^{i2\delta_{12}})e^{i2(\delta_{23}+\delta_{34})}-t_{2m}t'_{2m}t_{3m}t'_{3m}r_{1m}r_{4m}e^{i2(\delta_{12}+\delta_{23}+\delta_{34})}. \tag{11}$$

Missing coefficients G_{33} and G_{44} can be obtained from the above equations using $G_{33}=-(G_{34}+G_{31}+G_{32})$ and $G_{44}=-(G_{43}+G_{41}+G_{42})$. For calculating G^c, one furthermore needs

$$|S_{14}^m|=|D_m^{-1}t'_{1m}t'_{2m}t'_{3m}t'_{4m}|, \tag{12}$$

$$|S_{13}^m|=|D_m^{-1}t'_{1m}t'_{2m}||u_{3m}+r_{4m}e^{i2\delta_{34}}(t'_{3m}v_{3m}-r'_{3m}u_{3m})| \tag{13}$$

and

$$S_{11}^m-r'_{1m}=D_m^{-1}t_{1m}t'_{1m}e^{i2\delta_{12}}\{r_{2m}(1-r'_{3m}r_{4m}e^{i2\delta_{34}})+e^{i2\delta_{23}}[r_{3m}+r_{4m}e^{i2\delta_{34}}(t_{3m}t'_{3m}-r_{3m}r'_{3m})][t_{2m}t'_{2m}-r_{2m}r'_{2m}]\}. \tag{14}$$

The denominator D_m accounts for multiple reflections inside the CNT. Figure 3 depicts some resonances $\mathcal{A}_n^m$, with $n\in[1,6]$, which can occur in limiting cases where $t_{2[3],m}=t'_{2[3],m}=0$ or 1. In the general case, Eq. (11) indicates that these different resonances are coupled. For $t_{2m}=t'_{2m}=0$, G^c corresponds to the conductance of a two-terminal device, independent of δ_{23} and δ_{34}, and V^c vanishes. For $t_{2m}=t'_{2m}\neq 0$ and $t_{3m}=t'_{3m}=0$, G^c depends on δ_{12} and δ_{23}, but not on δ_{34}, and V^c still vanishes. Having a nonlocal signal $V^c\neq 0$ requires a direct CNT-CNT transmission at both contacts 2 and 3. It also requires that the four channels m are not coupled to the leads in the same way. Indeed, from Eqs. (3) and (8), one can check that if all the S_{jk}^m coefficients are independent of m, one finds $V^c=0$ due to the series structure of the device.[24] Interestingly, a finite V^c has already been

obtained in a CNT connected to four normal-metal leads,[12] which suggests that the K and K' modes were not similarly coupled to those leads. In principle, such an asymmetry is also possible with ferromagnetic contacts.

B. Parametrization of the lead/nanotube contacts

In the following, we assume that the top and bottom halves of the three terminals contacts $j \in \{2,3\}$ in Fig. 1 are symmetric. We furthermore take into account that the scattering matrix associated to each contact is invariant upon transposition due to spin conservation.[25] This gives $t_{jm}=t'_{jm}$, $r_{jm}=r'_{jm}$, and $u_{jm}=u'_{jm}=v_{jm}=v'_{jm}$ for $j \in \{2,3\}$. In this case, one can check from Eqs. (5)–(14) that G^c and V^c depend only on six interfacial scattering phases, i.e., those of r_{1m}, t_{2m}, r_{2m}, t_{3m}, r_{3m}, and r_{4m}, which correspond to processes during which electrons remain inside the CNT.[26] For contacts $j \in \{2,3\}$, it is thus convenient to use the parametrization

$$t_{j(p,\sigma)} = \sqrt{T_{j,p}(1+\sigma P_{j,p})}e^{i[\varphi^T_{j,p}+(\sigma/2)\Delta\varphi^T_{j,p}]}, \tag{15}$$

$$r_{j(p,\sigma)} = \Big[\sqrt{1-|t_{j(p,\sigma)}\sin[\phi_j^{(p,\sigma)}]|^2} + |t_{j(p,\sigma)}|\cos[\phi_j^{(p,\sigma)}]\Big]e^{i[\varphi^R_{j,p}+(\sigma/2)\Delta\varphi^R_{j,p}]}, \tag{16}$$

$$|u_{jm}| = \sqrt{1-|r_{jm}|^2-|t_{jm}|^2}, \tag{17}$$

with

$$\phi_j^{(p,\sigma)} = \varphi^R_{j,p} - \varphi^T_{j,p} + \frac{\sigma}{2}(\Delta\varphi^R_{j,p} - \Delta\varphi^T_{j,p}).$$

The above expressions depend on six real parameters $T_{j,p}$, $P_{j,p}$, $\varphi^T_{j,p}$, $\varphi^R_{j,p}$, $\Delta\varphi^R_{j,p}$, and $\Delta\varphi^T_{j,p}$ (Ref. 27). In order to have unitary lead/CNT scattering matrices, one must use $0 \le T_{j,p}(1+\sigma P_{j,p}) \le 1$ and $\pi/2 \le \phi_j^m[2\pi] \le 3\pi/2$.[28] These conditions imply that $0 \le |t_{jm}|^2 \le 1$, $0 \le |r_{jm}|^2 \le 1$, and $0 \le |u_{jm}|^2 \le 1/2$.[29] For contacts $j \in \{1,4\}$, one can use

$$|t_j^{(p,\sigma)}| = |t_j'^{(p,\sigma)}| = \sqrt{T_{j,p}(1+\sigma P_{j,p})} \tag{18}$$

and

$$\arg(r_j^{(p,\sigma)}) = c_p\varphi_j^R + \frac{\sigma}{2}\Delta\varphi^R_{j,p} \tag{19}$$

with $c_{K(K')} = \pm 1$. In Eq. (19), we have assumed $\Sigma_{p,\sigma}\arg(r_1^{(p,\sigma)})=0$ and $\Sigma_{p,\sigma}\arg(r_4^{(p,\sigma)})=0$ because, from Eqs. (5)–(14), these quantities only shift the variations of G^c, V^c, MG, and MV with respect to δ_{12} and δ_{34}, respectively. The parameters $P_{j,p}$, with $j \in \{1,2,3,4\}$, produce a spin polarization of the transmission probabilities $|t_j^m|^2$. The parameters $\Delta\varphi^{R(T)}_{j,p}$ allow to take into account the SDIPS, which has already been shown to affect significantly the behavior of CNT spin valves.[16–18] We will show below that the SDIPS also modifies the behavior of multiterminal setups. Note that for $j \in \{2,3\}$, the parameters $\Delta\varphi^{R(T)}_{p,j}$ also contribute to the spin dependence of $|r_{jm}|^2$ and $|u_{jm}|^2$: the SDIPS and the spin dependence of interfacial scattering probabilities are not independent in three-terminal contacts due to the unitarity of scattering processes.

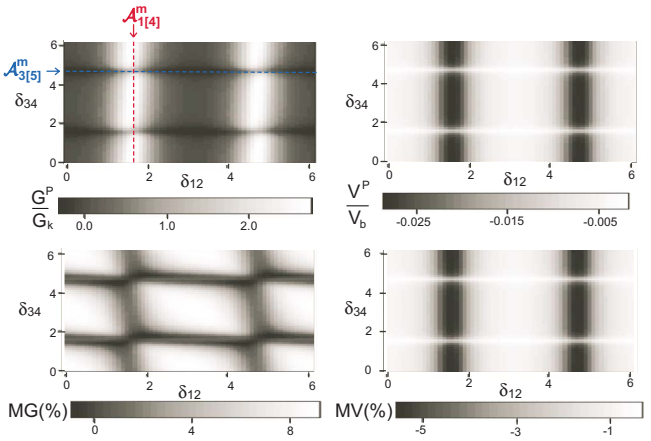

FIG. 4. (Color online) Signals G^P (top left panel), V^P (top right panel), MG (bottom left panel), and MV (bottom right panel) as a function of δ_{12} (horizontal axes) and δ_{34} (vertical axes) for a setup (a) with symmetric K and K' channels. We have used $T_{1,K[K']}=0.6$, $T_{2,K[K']}=0.1$, $T_{(3)4,K[K']}=0.3$, $P_{2[3],K[K']}=0.4$, $\varphi^R_{1(4)}=0$, $\varphi^R_{2(3),K[K']}=\pi$, $\varphi^T_{2[3],K[K']}=0$, $\Delta\varphi^{R\{T\}}_{2(3),K[K']}=0$, and $\delta_{23}=\pi$. We have indicated the position of the resonances $\mathcal{A}^m_{1(4)}$ and $\mathcal{A}^m_{3(5)}$ with red and blue dashed lines, respectively.

C. Behavior of setup (a)

We now consider setup (a), which has been frequently used in the MDI regime, for studying the spin-accumulation effect.[3–8] We first assume that the K and K' channels are coupled identically to the leads. This case is illustrated by Fig. 4, which shows the variations in G^P (top left panel), V^P (top right panel), MG (bottom left panel), and MV (bottom right panel) versus δ_{12} (horizontal axes) and δ_{34} (vertical axes). One can first notice that all these signals present strong variations with δ_{12} and δ_{34}, due to quantum interferences occurring inside the CNT. In Fig. 4, $G^P(\delta_{12})$ presents peaks which correspond to the resonances $\mathcal{A}^m_1$ (see, e.g., vertical dashed line) because we consider a case where T_{2m} is weak (these peaks also correspond accidentally to the resonances $\mathcal{A}^m_4$, which are much broader). A more remarkable result is that $G^P(\delta_{34})$ presents antiresonances which correspond to $\mathcal{A}^m_3$ and $\mathcal{A}^m_5$ (see, e.g., blue dashed line). This is a signature of the strongly nonlocal nature of current transport in this circuit: the electric signal measured in a given section of the CNT can be sensitive to resonances occurring in other sections of the CNT. We note that in Fig. 4, $|V^P|$ presents the same type of variations as G^P with δ_{12} and δ_{34}. In the general case, the resonances or antiresonances shown by the electric signals will not necessarily correspond to those defined in Fig. 3 due to the strong coupling between these different types of resonances. Importantly, we find that the MG signal can be finite, contrary to what happens in the MDI limit. Indeed, in Fig. 4, MG can exceed 8%. We note that in Fig. 4, MG presents minima approximately correlated with the maxima of G^P in the δ_{12} direction and with the minima of G^P in the δ_{34} direction. In the case of a S^m matrix independent from m, one finds $V^c=0$ (see Sec. IV). By continuity, since we have used in Fig. 4 relatively low values for $P_{2[3],K[K']}$, no SDIPS, and symmetric K and K' channels, we find $|V^P| \ll V_b$. More precisely, a lowest order development with re-

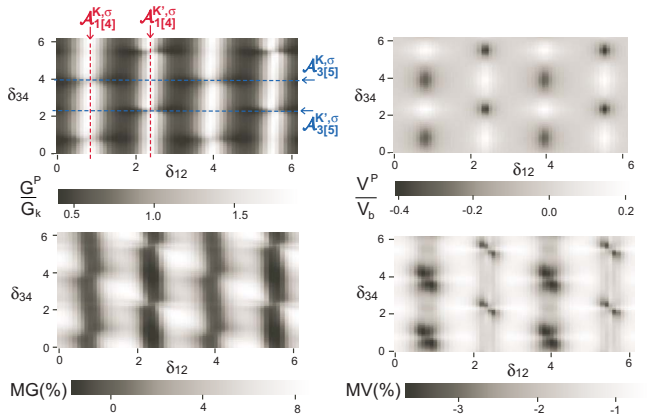

FIG. 5. (Color online) Signals G^P, V^P, MG, and MV as a function of δ_{12} and δ_{34} for setup (a) with dissymmetric K and K' channels. We have used $T_{1[4],K}=0.5$, $T_{1[4],K'}=0.3$, $T_{2,K[K']}=0.1$, $T_{3,K[K']}=0.3$, $P_{2[3],K[K']}=0.4$, $\varphi^R_{2(3),K[K']}=\pi$, $\varphi^T_{2[3],K[K']}=0$, $\varphi^R_{1(4)}=\pi/2$, $\Delta\varphi^{R\{T\}}_{2(3),K[K']}=0$, and $\delta_{23}=\pi$. We have indicated the position of the resonances $\mathcal{A}^m_{1(4)}$ and $\mathcal{A}^m_{3(5)}$ with red and blue dashed lines, respectively.

spect to P_2 and P_3 yields $V^P\sim -V^{\mathrm{AP}}\sim \lambda P_2 P_3$, with $\lambda \ll 1$, λ being a function of the different system parameters. In these conditions, MV presents the same type of variations as V^P (one has $MV\sim 2V^P$). When the K and K' modes are strongly asymmetric, it is possible to obtain a strong $|V^P/V_b|$ ratio for relatively low polarizations $P_{2[3],p}$. This case is illustrated by Fig. 5, where we have used $T_{1[4],K}\neq T_{1[4],K'}$ and $\varphi^R_{1(4)}\neq 0$ so that $\mathcal{A}^{(K,\sigma)}_{1[4]}\neq \mathcal{A}^{(K',\sigma)}_{1[4]}$ and $\mathcal{A}^{(K,\sigma)}_{3[5]}\neq \mathcal{A}^{(K',\sigma)}_{3[5]}$. In this case, the variations shown by the different electric signals are more complicated than previously. However, we find $V^P\sim V^{\mathrm{AP}}$ so that the amplitude of MV remains comparable to that of Fig. 4.

We now discuss the signs of the different signals. We have already seen above that with the parameters of Fig. 4, one has $V^P>0$ and $V^{\mathrm{AP}}<0$. In other conditions, it is possible to have $V^P<0$ and $V^{\mathrm{AP}}>0$, or V^P and V^{AP} both positive or both negative (not shown). In the CFC model, the signs of V^P and V^{AP} are thus independent, whereas MDI models usually give opposite signs for V^P and V^{AP} [see, e.g., Eq. (21) of the Appendix and Refs. 30 and 31]. Figure 5 illustrates that there exist sets of parameters such that the nonlocal voltage V^P changes sign while sweeping δ_{12} or δ_{34} (this result is also true for δ_{23}).[32] It is also possible to find sets of parameters such that MV (not shown) and MG (see Fig. 6, bottom left panel, full lines) change signs with δ_{12}, δ_{23}, or δ_{34}.

We now briefly discuss the effects of the contact polarizations. One can generally increase the amplitude of the magnetic signals by increasing $P_{j,p}$ (not shown), $|\Delta\varphi^R_{j,p}|$ (see Fig. 6, red full lines), and $|\Delta\varphi^T_{j,p}|$ (not shown). A strong SDIPS can split the resonances or antiresonances of the electric signals (not shown), similarly to what has been found in the two-terminal $F/\mathrm{CNT}/F$ case.[16] Interestingly, in the case of a two-terminal $F/\mathrm{CNT}/F$ device with a $K-K'$ degeneracy and no SDIPS (using $1=F$, $2=F$, and no leads 3 and 4), Ref. 16 has found that the oscillations of MG with δ_{12} are symmetric and a finite SDIPS is necessary to break this symmetry. In contrast, in setup (a), the oscillations of $MG(\delta_{12})$ can be

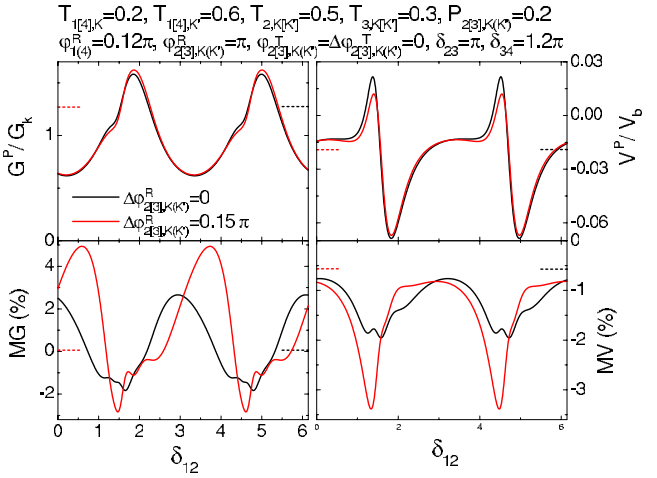

FIG. 6. (Color online) Signals G^P, V^P, MG, and MV as a function of δ_{12} for setup (a). We consider a case with no SDIPS (black lines) and a case with a finite SDIPS (red lines corresponding to $\Delta\varphi^R_{2(3),K[K']}=0.15\pi$). We have used $T_{1[4],K}=0.2$, $T_{1[4],K'}=0.6$, $T_{2,K[K']}=0.5$, $T_{3,K[K']}=0.3$, $P_{2[3],K[K']}=0.2$, $\varphi^R_{1(4)}=0.12\pi$, $\varphi^R_{2(3),K[K']}=\pi$, $\varphi^T_{2[3],K[K']}=\Delta\varphi^T_{2(3),K[K']}=0$, $\delta_{23}=\pi$, and $\delta_{34}=0.12\pi$. The full lines correspond to the CFC prediction (Sec. IV), and the dotted lines to the IFC prediction (Sec. V). The second does not depend on δ_{12}. In the IFC case, the MG signal is hardly visible in this figure because it is of the order of 0.06%.

asymmetric in spite of the $K-K'$ degeneracy and the absence of a SDIPS (see Fig. 6, bottom left panel).

D. Behavior of setup (b)

In setup (b), the types of resonances or antiresonances shown by the electric signals depend again on the value of the coupling between the different CNT sections. We will only highlight the most interesting specificities of setup (b) because it has many common properties with setup (a). Figure 7 shows, with black (red) full lines, examples of $G^P(\delta_{12})$, $MG(\delta_{12})$, $V^P(\delta_{12})$, and $MV(\delta_{12})$ curves for symmetric (asymmetric) K and K' channels. Strikingly, in both cases, the magnetoconductance MG between N leads 1 and 2 can be finite, although the two F leads are located outside the classical current path. This is in strong contrast with the MDI limit. From Eqs. (3) and (8), the voltage difference V^c vanishes if the scattering properties of contacts 1 or 2 are independent of the transverse index p, regardless of the scattering properties of contacts 3 and 4.[33] This leads to the paradoxical situation where a magnetic signal can be measured between the two N leads but not between the two F leads (see black full lines in Fig. 7). By continuity, when the $K-K'$ asymmetry is not large at contacts 1 and 2, the amplitude of the signals V^P and MV measured between contacts 3 and 4 will remain very small. It is possible to obtain stronger amplitudes for V^c and MV in the opposite limit of strongly asymmetric K and K' channels (see red full lines in Fig. 7 for which we have used $\varphi_{2,K}\neq\varphi_{2,K'}$). With setup (b), it is thus also possible to obtain magnetic signals in both G^c and V^c, whereas MG and MV would vanish in the MDI limit.

E. Comparison with the MDI limit

In this section, we summarize the most striking differences between the CFC model of Sec. IV and the MDI model

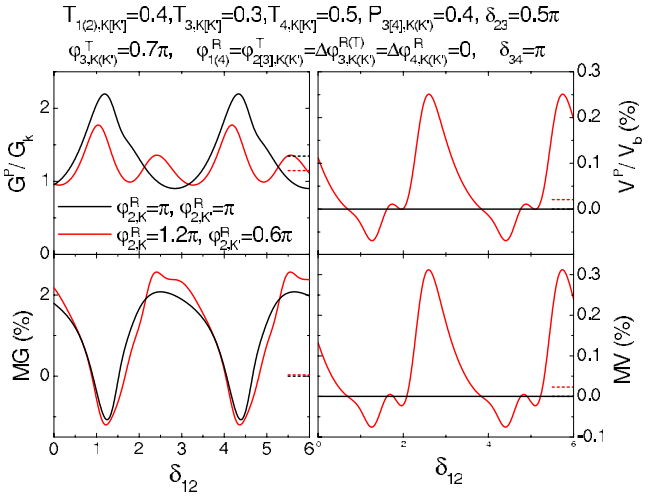

FIG. 7. (Color online) Signals G^P, V^P, MG, and MV as a function of δ_{12}, for setup (b). The black (red) lines correspond to the cases of K and K' channels coupled identically (differently) to the contacts, i.e., $\varphi^R_{2,K}=\varphi^R_{2,K'}=\pi(\varphi^R_{2,K}=1.2\pi,\varphi^R_{2,K'}=0.6\pi)$. We have used $T_{1[2],K(K')}=0.4$, $T_{3,K[K']}=0.3$, $T_{4,K[K']}=0.5$, $P_{3[4],K[K']}=0.4$, $\varphi^R_{1(4)}=\varphi^T_{2(3),K[K']}=\Delta\varphi^{R(T)}_{3,K[K']}=\Delta\varphi^R_{4,K[K']}=0$, $\delta_{23}=\pi/2$, and $\delta_{34}=\pi$. The full lines correspond to the CFC prediction and the dotted lines to the IFC prediction. In the black case, the MG signal vanishes in the IFC limit, and the V^P and MV signals vanish in both the IFC and CFC limits. The MG signal of the red case is hardly visible in the IFC limit because it is of the order of 0.03%.

of Sec. III. For setup (b), the CFC model allows $V^P\neq 0$ and $MV\neq 0$ whereas one finds $V^P=0$ and $MV=0$ with the MDI model. Another remarkable result is that for both setups (a) and (b), the CFC model gives $G^P\neq G^{\mathrm{AP}}$ whereas the MDI model imposes $G^P=G^{\mathrm{AP}}$. The table in Fig. 1 summarizes these results.

V. INCOHERENT FOUR-CHANNEL LIMIT

In order to determine whether the specific spin-dependent behavior of the CFC model is due to coherence or to the low number of channels, it is interesting to consider the IFC limit. If the phase relaxation length of the CNT is much shorter than the distance between the different contacts, the global transmission and reflection probabilities of setups (a) and (b) can be calculated by composing the scattering probabilities of the different contacts instead of the scattering amplitudes.[34] We have checked that this leads to replacing the scattering probabilities $|S^m_{\alpha\beta}(\{r_{jm},t_{jm},v_{jm},u_{jm},\delta_{ij}\})|^2$ occurring in Eqs. (1) and (2) by $S^m_{\alpha\beta}(\{|r_{jm}|^2,|t_{jm}|^2,|v_{jm}|^2,|u_{jm}|^2,0\})$. Importantly, this description remains intrinsically quantum since the channel quantization is taken into account. In Figs. 6 and 7, we show with black and red dotted lines the IFC values corresponding to the different CFC curves. We find that G^c, V^c, MG, and MV do not depend anymore on the phases δ_{ij}. However, $G^P\neq G^{\mathrm{AP}}$ is still possible for setups (a) and (b). More precisely, we have checked analytically that using identical K and K' modes leads to[33] $G^P=G^{\mathrm{AP}}$, and we have checked numerically that $G^P\neq G^{\mathrm{AP}}$ occurs in the case of a K/K' asymmetry at one of the four contacts for setup (a) and at contacts 1 or 2 for setup (b). We can also obtain $V^P\neq 0$ and $MV\neq 0$ for setup (b) [and, more trivially, for setup (a)], with the same symmetry restrictions as for the CFC case (see table in Fig. 1). Therefore, having $V^P\neq 0$ and $MV\neq 0$ for setup (b) and $MG\neq 0$ for setups (a) and (b) is not a specificity of the coherent case: using a very small number of transport channels already allows these properties. It is nevertheless important to notice that the values of MG and MV are strongly enhanced in the CFC case due to resonance effects. Moreover, in the IFC case, the circuit is insensitive to the SDIPS, whereas in the coherent case, the SDIPS further increases the amplitude of MV and MG.[35] At last, the coherent case presents the interest of allowing strong variations in the electric signals with the gate-controlled phases δ_{12}, δ_{23}, and δ_{34}.

VI. DISCUSSION ON FIRST EXPERIMENTS

Reference 13 reports on a single wall carbon nanotube (SWNT) circuit biased like in Fig. 1 but with four ferromagnetic leads. A hysteretic V^c has been measured by flipping sequentially the magnetizations of the two inner contacts. However, no conclusion can be drawn from this experiment due to the lack of information on the conduction regime followed by the device. Reference 14 reports on V^c measurements for setup (a) made with a SWNT. Gunnarsson *et al.*[14] observed a finite V^c which oscillates around zero while the back-gate voltage of the sample is swept. This suggests that this experiment was in the coherent regime. However, the amplitude of V^c was very low $[\max(|V^c/V_b|)\sim 0.01]$, which indicates—in the framework of the scattering model—that the K and K' modes were very close and the spin polarization of the contacts scattering properties was very weak. It is therefore not surprising that Gunnarsson *et al.*[14] did not obtain a measurable MV signal. Although setup (a) seems very popular in the nanospintronics community for historical reasons,[3] we have shown above that setup (b) also highly deserves an experimental effort, as well as MG measurements in general.

In this article, we have chosen to focus on the case of double mode quantum wires because this is adapted for describing CNT-based devices, which are presently among the most advanced nanospintronics devices. However, technological progress might offer the opportunity to observe the effects depicted in this article in other types of nanowires, such as, e.g., semiconducting nanowires. Indeed, quantum interferences have already been observed in Si (Ref. 36) and InAs quantum wires,[37] and spin injection has already been demonstrated in Si layers[38] and InAs quantum dots.[39] One major difficulty may consist in reaching the few modes and fully ballistic[40] regime with these devices.

VII. CONCLUSION

In this work, we have studied theoretically various circuits consisting of a carbon nanotube with two transverse modes, contacted to two normal-metal leads and two ferromagnetic leads. Two contacts are used as source and drain to define a local conductance, and the two other contacts are

left floating, to define a nonlocal voltage outside the classical current path. When the magnetizations of the two ferromagnetic contacts are changed from a parallel to an antiparallel configuration, we predict, in the local conductance and the nonlocal voltage, magnetic signals which are specific to the case of a system with a low number of channels. In particular, we propose an arrangement of the normal and ferromagnetic leads [setup (b)] which would give no magnetic response in the MDI limit but which allows magnetic responses in both the local conductance and the nonlocal voltage in the two-mode regime. The more traditional arrangement [setup (a)] used for the study of the MDI limit also shows a qualitatively different behavior, i.e., a magnetic response in the local conductance. These specific magnetic behaviors are strongly reinforced in the coherent case due to resonance effects occurring inside the nanotube and also, possibly, due to the spin dependence of interfacial phase shifts. Our calculations pave the way for experiments on nonlocal spin transport in low-dimensional conductors.

ACKNOWLEDGMENTS

We acknowledge discussions with H. U. Baranger and G. E. W. Bauer. This work was financially supported by the ANR under Contract No. 05-NANO-055, the European Union under Contract No. FP6-IST-021285-2, and the C'Nano Ile de France contract SPINMOL. We acknowledge the hospitality of STCM-Kyoto organized by YIPQS program at Yukawa Institute for Theoretical Physics.

APPENDIX: DISCUSSION OF THE MDI LIMIT WITH A RESISTORS NETWORK

In this appendix, we discuss the MDI regime with an elementary but insightful resistors network model. When the electronic mean-free path is much shorter than the spin-flip length, it is possible to define a spin-dependent electrochemical potential which obeys a local spin-dependent Ohm's law.[20] Thus, neglecting spin-flip scattering inside the CC, one can use the effective resistor network of Fig. 8 to describe the behaviors of setups (a) and (b) in the MDI limit.[13,19] For completeness, we allow the four leads $j \in \{1,2,3,4\}$ to be ferromagnetic, with collinear magnetizations. The left (right) part of the resistors network corresponds to the up (down) spin channel. Due to intralead spin-flip scattering, electrons are in local equilibrium in lead j. This equilibration is described by the electrical connection of $\uparrow$ and $\downarrow$ channels at node j, which has an electric potential V_j^c. The section $j-k$ of the CC is modeled with the two resistors R_{jk}. The contact between lead j and the CC is represented by the resistors R_j^σ, r_j^σ, and $\tilde{r}_j^\sigma$. When lead j is not ferromagnetic, one must use $R_j^\uparrow = R_j^\downarrow$, $r_j^\uparrow = r_j^\downarrow$, and $\tilde{r}_j^\uparrow = \tilde{r}_j^\downarrow$. The current flowing from lead 1 to lead 2 is $I_1^c = I_{1\uparrow}^c + I_{1\downarrow}^c$. Since leads 3 and 4 are floating, they supply the CC with spin currents which are perfectly equilibrated, i.e., $I_{j\uparrow} = -I_{j\downarrow}$ for $\alpha \in \{3,4\}$. We find

$$G^c = \mathcal{H} V_b / \mathcal{D} \tag{20}$$

and

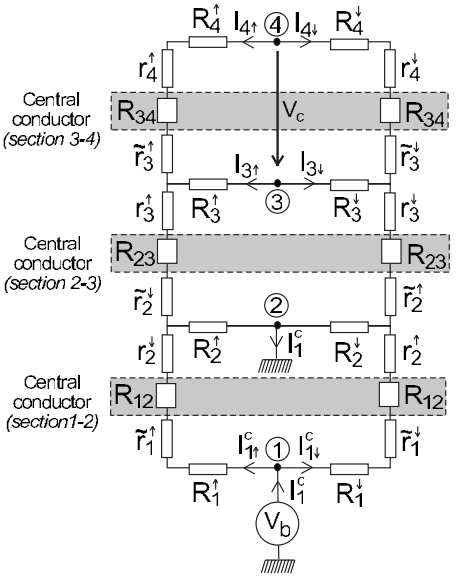

FIG. 8. Resistors network used to describe the behavior of a CC connected to four leads $j \in \{1,2,3,4\}$ in the MDI limit. The contact between lead j and the CC is represented by the resistors R_j^σ, r_j^σ, and $\tilde{r}_j^\sigma$. The section $j-k$ of the CC is modeled with the two resistors R_{jk}. When lead j is not ferromagnetic, one must use $R_j^\uparrow = R_j^\downarrow$, $r_j^\uparrow = r_j^\downarrow$, and $\tilde{r}_j^\uparrow = \tilde{r}_j^\downarrow$.

$$V^c = (A_{34}^\uparrow - A_{34}^\downarrow)(B_{12}^\uparrow - B_{12}^\downarrow) V_b / \mathcal{R}_{23} \mathcal{H} \tag{21}$$

with

$$\mathcal{R}_{23} = \frac{R_3^\uparrow + R_3^\downarrow}{\sum_\sigma (\mathcal{R}_{34}^\sigma - R_3^\sigma)} + \sum_\sigma (\tilde{r}_2^\sigma + r_3^\sigma + R_{23}) \tag{22}$$

$$\mathcal{H} = \sum_\sigma (\mathcal{R}_{12}^\sigma + \alpha_{\sigma,\sigma} + \alpha_{\sigma,-\sigma}) \tag{23}$$

$$\mathcal{D} = (\mathcal{R}_{12}^\uparrow + \alpha_{\uparrow,\uparrow})(\mathcal{R}_{12}^\downarrow + \alpha_{\downarrow,\downarrow}) - \alpha_{\uparrow,\downarrow}\alpha_{\downarrow,\uparrow} \tag{24}$$

$$2A_{34}^\sigma = \mathcal{R}_{34}^\sigma [(R_3^\uparrow + R_3^\downarrow)/(\mathcal{R}_{34}^\uparrow + \mathcal{R}_{34}^\downarrow)] - R_3^\sigma \tag{25}$$

$$B_{12}^\sigma = (\mathcal{R}_{12}^\sigma + \alpha_{\sigma,\sigma} + \alpha_{-\sigma,\sigma})(\mathcal{R}_{12}^{-\sigma} - R_2^{-\sigma}) \tag{26}$$

$$\alpha_{\sigma,\sigma'} = R_2^\sigma (\mathcal{R}_{12}^{\sigma'} - R_2^{\sigma'}) / \mathcal{R}_{23} \tag{27}$$

and

$$\mathcal{R}_{jk}^\sigma = R_j^\sigma + \tilde{r}_j^\sigma + R_k^\sigma + r_k^\sigma + R_{jk} \tag{28}$$

for $(j,k) \in \{1,2,3,4\}^2$. The value of $\mathcal{H}$ is independent of the contacts magnetic configuration, but $\mathcal{D}$ depends on the relative configuration of leads 1 and 2 so that $G^P \neq G^{AP}$ is possible provided leads 1 and 2 are ferromagnetic. In contrast, the value of G^c is independent of the magnetization directions of leads 3 or 4 because, due to $I_{3(4)\uparrow} = -I_{3(4)\downarrow}$, the resistors R_3^σ, r_3^σ, $\tilde{r}_3^\sigma$, R_4^σ, and r_4^σ of Fig. 8 are connected in series with $R_3^{-\sigma}$, $r_3^{-\sigma}$, $\tilde{r}_3^{-\sigma}$, $R_4^{-\sigma}$, and $r_4^{-\sigma}$, respectively. We conclude that for setups (a) and (b), one has $G^P = G^{AP}$ in the MDI limit. From Eq. (21), having $V^P \neq 0$ requires that at least one of

biased leads 1 or 2 is ferromagnetic (for the generation of a spin accumulation) and at least one of floating leads 3 or 4 is ferromagnetic (for the detection of this spin accumulation). These conditions are fulfilled for setup (a) but not for setup (b). Importantly, these results will not be modified if a moderate intra-CC spin-flip scattering or the finite width of the contacts is taken into account because both features can be modeled with a distributed array of resistors connecting the two spin branches, which will not change the spin symmetry of the model in Fig. 8.

[1] C. P. Umbach, P. Santhanam, C. van Haesendonck, and R. A. Webb, Appl. Phys. Lett. **50**, 1289 (1987).

[2] A. Benoit, C. P. Umbach, R. B. Laibowitz, and R. A. Webb, Phys. Rev. Lett. **58**, 2343 (1987); W. J. Skocpol, P. M. Mankiewich, R. E. Howard, L. D. Jackel, D. M. Tennant, and A. D. Stone, *ibid.* **58**, 2347 (1987).

[3] M. Johnson and R. H. Silsbee, Phys. Rev. Lett. **55**, 1790 (1985).

[4] F. J. Jedema, A. T. Filip, and B. J. van Wees, Nature (London) **410**, 345 (2001).

[5] F. J. Jedema, H. B. Heersche, A. T. Filip, J. J. A. Baselmans, and B. J. van Wees, Nature (London) **416**, 713 (2002).

[6] M. Zaffalon and B. J. van Wees, Phys. Rev. B **71**, 125401 (2005).

[7] X. Lou, C. Adelmann, S. A. Crooker, E. S. Garlid, J. Zhang, K. S. M. Reddy, S. D. Flexner, C. J. Palmstrom, and P. A. Crowell, Nat. Phys. **3**, 197 (2007).

[8] N. Tombros, C. Jozsa, M. Popinciuc, H. T. Jonkman, and B. J. van Wees, Nature (London) **448**, 571 (2007).

[9] R. H. Silsbee, Bull. Magn. Reson. **2**, 284 (1980).

[10] W. Liang, M. Bockrath, D. Bozovic, J. H. Hafner, M. Tinkham, and H. Park, Nature **411**, 665 (2001); M. R. Buitelaar, A. Bachtold, T. Nussbaumer, M. Iqbal, and C. Schönenberger, Phys. Rev. Lett. **88**, 156801 (2002); D. Mann, A. Javey, J. Kong, Q. Wang, and H. Dai, Nano Lett. **3**, 1541 (2003); J. Cao, Q. Wang, M. Rolandi, and H. Dai, Phys. Rev. Lett. **93**, 216803 (2004); H. T. Man, I. J. W. Wever, A. F. Morpurgo, Phys. Rev. B **73**, 241401(R) (2006); K. Grove-Rasmussen, H. I. Jørgensen, and P. E. Lindelof, Physica E **40**, 92 (2007); L. G. Herrmann, T. Delattre, P. Morfin, J.-M. Berroir, B. Plaçais, D. C. Glattli, and T. Kontos, Phys. Rev. Lett. **99**, 156804 (2007).

[11] A. Cottet, T. Kontos, S. Sahoo, H. T. Man, M.-S. Choi, W. Belzig, C. Bruder, A. F. Morpurgo, and C. Schönenberger, Semicond. Sci. Technol. **21**, S78 (2006).

[12] A. Makarovski, A. Zhukov, J. Liu, and G. Finkelstein, Phys. Rev. B **76**, 161405(R) (2007).

[13] N. Tombros, S. J. van der Molen, and B. J. van Wees, Phys. Rev. B **73**, 233403 (2006).

[14] G. Gunnarsson, J. Trbovic, and C. Schönenberger, Phys. Rev. B **77**, 201405(R) (2008).

[15] W. Liang, M. Bockrath, and H. Park, Phys. Rev. Lett. **88**, 126801 (2002); B. Babić and C. Schönenberger, Phys. Rev. B **70**, 195408 (2004); P. Jarillo-Herrero, J. Kong, H. S. J. van der Zant, C. Dekker, L. P. Kouwenhoven, and S. De Franceschi, Phys. Rev. Lett. **94**, 156802 (2005); S. Moriyama, T. Fuse, M. Suzuki, Y. Aoyagi, and K. Ishibashi, *ibid.* **94**, 186806 (2005); S. Sapmaz, P. Jarillo-Herrero, J. Kong, C. Dekker, L. P. Kouwenhoven, and H. S. J. van der Zant, Phys. Rev. B **71**, 153402 (2005).

[16] A. Cottet, T. Kontos, W. Belzig, C. Schönenberger, and C. Bruder, Europhys. Lett. **74**, 320 (2006).

[17] A. Cottet and M.-S. Choi, Phys. Rev. B **74**, 235316 (2006).

[18] S. Sahoo, T. Kontos, J. Furer, C. Hoffmann, M. Gräber, A. Cottet, and C. Schönenberger, Nature Phys. **1**, 99 (2005).

[19] T. Valet and A. Fert, Phys. Rev. B **48**, 7099 (1993).

[20] I. Žutić, J. Fabian, and S. Das Sarma, Rev. Mod. Phys. **76**, 323 (2004).

[21] M. Büttiker, Phys. Rev. Lett. **57**, 1761 (1986).

[22] R. Saito, G. Dresselhaus, and M. S. Dresselhaus, *Physical Properties of Carbon Nanotubes* (Imperial College Press, London, 1998).

[23] N. Mason, M. J. Biercuk, and C. M. Marcus, Science **303**, 655 (2004); M. R. Gräber, W. A. Coish, C. Hoffmann, M. Weiss, J. Furer, S. Oberholzer, D. Loss, and C. Schönenberger, Phys. Rev. B **74**, 075427 (2006).

[24] H. U. Baranger, Phys. Rev. B **42**, 11479 (1990).

[25] Spin conservation allows mapping of the scattering description of each spin component $\sigma \in \{\uparrow, \downarrow\}$ onto a spinless problem. Time-reversal symmetry in each of these spinless problems implies $t_{jm}=t'_{jm}$, $u_{jm}=u'_{jm}$, and $v_{jm}=v'_{jm}$.

[26] From Eq. (14), the phase of $t_{1m}t'_{1m}/r'_{1m}$ can also affect signals G^c and V^c. However, since the scattering matrix of contact 1 is unitary, one finds $t_{1m}t'_{1m}/r'_{1m}=-r_{1m}|t_{1m}/r_{1m}|^2$. It is thus sufficient to use $\arg(r_{1m})$ as a parameter.

[27] The complete parametrization of the scattering matrices of contacts $j \in \{2,3\}$ requires extra parameters $\varphi^U_{j,p}$, and $\Delta\varphi^U_{j,p}$ such that $\arg(u_{j(p,\sigma)})=\varphi^U_{j,p}+\sigma\Delta\varphi^U_{j,p}/2$ and $r''_{jm}=-(1-2|u_{jm}|^2)^{1/2}e^{i\arg[(u_{jm})^2/(A^m_j+B^m_j)]}$. However, one can check that, with the assumptions made in Sec. IV B, signals G^c and V^c are independent of $\varphi^U_{j,p}$ and $\Delta\varphi^U_{j,p}$ for both setups (a) and (b).

[28] For completeness, we point out that the condition on ϕ^m_j can be relaxed if $t^m_j=0$.

[29] For $j \in \{2,3\}$, one has $|u_{jm}|^2 \leq 1/2$ because we assume that an electron arriving from contact j enters the top and bottom portions of the CNT with the same probabilities.

[30] M. Johnson and R. H. Silsbee, Phys. Rev. B **37**, 5312 (1988).

[31] S. Takahashi and S. Maekawa, Phys. Rev. B **67**, 052409 (2003).

[32] We find that the sign changes of V^P can already occur in the spin-degenerate case. Accordingly, a change in sign of V^P has already been observed for a CNT with four normal-metal leads by sweeping the CNT back-gate voltage (Ref. 12).

[33] We have checked analytically that this property is true even when contacts 2 and 3 are spatially asymmetric, i.e., $u_{(2)3m} \neq v_{(2)3m}$.

[34] S. Datta, *Electronic Transport in Mesoscopic Systems* (Cambridge University Press, Cambridge, 1995).

[35] In the IFC case, MV and MG are sensitive to the $\Delta\varphi^{R[T]}_{2(3),p}$ parameters through the reflection probabilities of contacts 2 and 3 but not through the scattering phases.

[36] A. T. Tilke, F. C. Simmel, H. Lorenz, R. H. Blick, and J. P. Kotthaus, Phys. Rev. B **68**, 075311 (2003).

[37] Y.-J. Doh, A. L. Roest, E. P. A. M. Bakkers, S. De Franceschi, and L. P. Kouwenhoven, J. Korean Phys. Soc. **54**, 135 (2009).
[38] B. T. Jonker, G. Kioseoglou, A. T. Hanbicki, C. H. Li, and P. E. Thompson, Nat. Phys. **3**, 542 (2007).
[39] K. Hamaya, M. Kitabatake, K. Shibata, M. Jung, M. Kawamura, K. Hirakawa, T. Machida, S. Ishida, and Y. Arakawa, Appl. Phys. Lett. **91**, 022107 (2007); K. Hamaya, S. Masubuchi, M. Kawamura, T. Machida, M. Jung, K. Shibata, K. Hirakawa, T. Taniyama, S. Ishida, and Y. Arakawa, *ibid.* **90**, 053108 (2007).
[40] X. Zhou, S. A. Dayeh, D. Aplin, D. Wang, and E. T. Yu, Appl. Phys. Lett. **89**, 053113 (2006).